

Article

M₆O₄(OH)₄ of M = Sn, Pb: Single Crystal Growth and Crystal Structure Determinations Far Away from Routine

Hans Reuter , Dirk Schröder and Kristina Peckskamp

Chemistry, Department of Biology/Chemistry, Osnabrück University, Barbarastr. 7, D-49069 Osnabrück, Germany
* Correspondence: hreuter@uos.de

Abstract: Single crystals of Sn₆O₄(OH)₄ have been grown over a period of more than a decade in hermetically sealed flasks of various triorganotin(IV)-trihydrides in toluene/*N,N*-dimethylformamide and those of Pb₆O₄(OH)₄ on a petri dish within some days from the reaction of Pb(ClO₄)₂ with Sr(OH)₂·8H₂O. High-resolution X-ray diffraction data of the tetragonally crystallizing compounds have been collected conventionally at 100 K. Crystal structure determinations have been performed in space groups *P4/mnc* and *P4̄2₁c* with different structure models because of a pretended specific systematic extinction condition. Its violation was routinely overseen because of the very low intensities of the respective reflections, an effect reinforced by crystal size. The non-existence of this systematic extinction was experimentally confirmed by studying the datasets in more detail, including the simulation of layer photographs. The importance of additional information obtained from dataset analysis tools and structure validation programs to assess the different structure models is demonstrated. Structures of both molecules are analyzed with respect to the molecules as a whole as well as to their constructive building units: two crystallographic different prototypes of {MO₄} coordination polyhedra with a bent seesaw conformation, one μ₃-OH- and one μ₃-O- group, each trigonal-pyramidally coordinated.

Keywords: crystal growth; systematic extinction condition; space group determination; refinement strategies; structure validation; building units; coordination polyhedra



Citation: Reuter, H.; Schröder, D.; Peckskamp, K. M₆O₄(OH)₄ of M = Sn, Pb: Single Crystal Growth and Crystal Structure Determinations Far Away from Routine. *Crystals* **2023**, *13*, 739. <https://doi.org/10.3390/cryst13050739>

Academic Editor: Ana M. Garcia-Deibe

Received: 31 March 2023

Revised: 24 April 2023

Accepted: 26 April 2023

Published: 27 April 2023



Copyright: © 2023 by the authors. Licensee MDPI, Basel, Switzerland. This article is an open access article distributed under the terms and conditions of the Creative Commons Attribution (CC BY) license (<https://creativecommons.org/licenses/by/4.0/>).

1. Introduction

The chemistry of bivalent tin and lead in aqueous solution is characterized by complicated equilibria between different mono- and polynuclear, cationic, or anionic *isopolyoxohydroxo* species of general formula [M^{II}_nO_o(OH)_p(H₂O)_q]^{(2n-2o-p)±} in amounts strongly depending on salt concentration and pH value. The knowledge of the species present in such a solution is of great importance, especially for Pb²⁺, as it is an environmental pollutant toxic to human species. While detailed insights into these equilibria come from potentiometric studies (pot, M = Sn [1], M = Pb [2]), accurate structural information about the species formed results from single crystal X-ray structure determinations (SCXRD) of crystals isolated from the solutions under appropriate conditions.

Although there are some discrepancies among authors about the different species formed, there is a great consensus that in strongly acidic solutions of Sn(II), the mononuclear dication [Sn(OH₂)₃]²⁺ (pot, SCXRD [3]) and monocation [Sn(OH)(OH₂)₂]⁺ (pot) dominate. Less acidic solutions predominantly contain the trinuclear tin-oxygen cluster [Sn₃(OH)₄]²⁺ (pot, SCXRD [4]), while in alkaline solutions, the dinuclear [Sn₂O(OH)₄]²⁻ (pot, SCXRD [5]) and mononuclear [Sn(OH)₃]⁻ (pot, SCXRD [5]) anions have been postulated and structurally characterized.

For Pb²⁺ mononuclear, hydrated species are less favorable because of their lower charge density [6] in comparison with Sn²⁺, but in less acidic solutions, the tetranuclear [Pb₄(OH)₄]²⁺ (pot, SCXRD [7–11]) and hexanuclear [Pb₆O(OH)₆]⁴⁺ (pot, SCXRD [12,13]) species are found. For alkaline solutions, the mononuclear anions [Pb(OH)₃]⁻ and [Pb(OH)₄]²⁻ (pot) have

been postulated. Despite these differences, both metals, tin and lead, form in neutral solution a less soluble, hexanuclear molecular *isopolyoxohydroxo* compound of composition $M_6O_4(OH)_4$.

Besides these chemical aspects, the tin compound is of some interest in archaeology, as $Sn_6O_4(OH)_4$ is often found as a thin, microcrystalline crust on tin or pewter artifacts. First described in 1971 and named *hydroromarchite*, the compound was classified as an anthropogenic mineral according to its formation in the context of human activities—“a canoe was overturned near Boundary Falls, Winnipeg, Ontario, and pannikins of its load submerged 15 feet below the surface of the water for more than a century” [14]. Later on, the mineral was also identified on historical tin objects found in seawater and soil [15–17]. In the mineral classification scheme of Strunz [18], *hydroromarchite*, Hrom [19], belongs to the subclass “FF Hydroxides with OH, without H_2O ; Various Polyhedra” of class 4 “Oxides”. In addition to its anthropogenic formation, there are also some indications that $Sn_6O_4(OH)_4$ may also occur under typical geochemical conditions [20]. Similar anthropogenic or natural findings of $Pb_6O_4(OH)_4$ are not yet documented.

Up until now, our knowledge about the molecular structures of both compounds has suffered from a lack of single crystals of suitable size and quality for single-crystal X-ray diffraction. Thus far, structural data are only based on room-temperature X-ray ($M = Sn$) [21] and neutron ($M = Pb$) [22] data, both from powder samples via Rietveld refinement. These calculations have been performed assuming that the compounds are isostructurally crystallizing in the primitive tetragonal, non-centrosymmetric space group $P\bar{4}2_1c$ (no. 114 [23]). While the structural data (bond lengths, bond angles, and hydrogen bonds) of the lead compound result from a conclusive structure model, those of the tin compound are very unprecise and less plausible, especially with respect to the tin-oxygen distances.

2. Materials and Methods

2.1. Chemical Background of Crystal Growth

The single crystals of this study have been found by chance as a result of two uncommon reactions: the reductive splitting of a tin-carbon bond of *organotin(IV) trihydrides* and the reaction of an aqueous lead(II) acetate solution with solid strontium hydroxide octahydrate.

$Sn_6O_4(OH)_4$. A lot of well-shaped, large, colorless single crystals (Figure 1) of the tin compound have been grown over more than a decade from solutions of various *monoorganotin(IV) trihydrides*, R_3SnH_3 , in mixtures of toluene and *N,N*-dimethylformamide, DMF. These samples were originally prepared to get monoorganotin(IV) clusters, $(RSn)_n$, via hydrogen elimination in DMF, a reaction well established [24–26] in the case of *triorganotin(IV) hydrides*, R_3SnH , and *diorganotin(IV) dihydrides*, R_2SnH_2 , resulting in the formation of *hexaorganodistannanes*, $(R_3Sn)_2$ [27], and *diorgano-cyclo-polystannanes*, $(R_2Sn)_n$ [28], respectively. From a chemical point of view, some aspects of the formation of $Sn_6O_4(OH)_4$ under these experimental conditions are unusual: (i) the reduction of the four-valent tin atoms in the *trihydrides* to bivalent ones in the title compound; (ii) the cleavage of the carbon-tin bonds; and (iii) the origin of oxygen. As the well-closed flasks with the *trihydrides* preserved their red color over the complete time of storage without fading but bleached within some hours when coming into contact with air, the origin of oxygen in the title compound from O_2 can be excluded. More likely, the oxygen content results from traces of water still present after drying the reaction solutions of the *trihydrides* conventionally with sodium sulfate. A possible reaction equation is sketched out in Scheme 1.



Scheme 1. Possible reaction equation for the formation of $Sn_6O_4(OH)_4$ from *triorganotin(IV) hydrides* in the presence of traces of water.

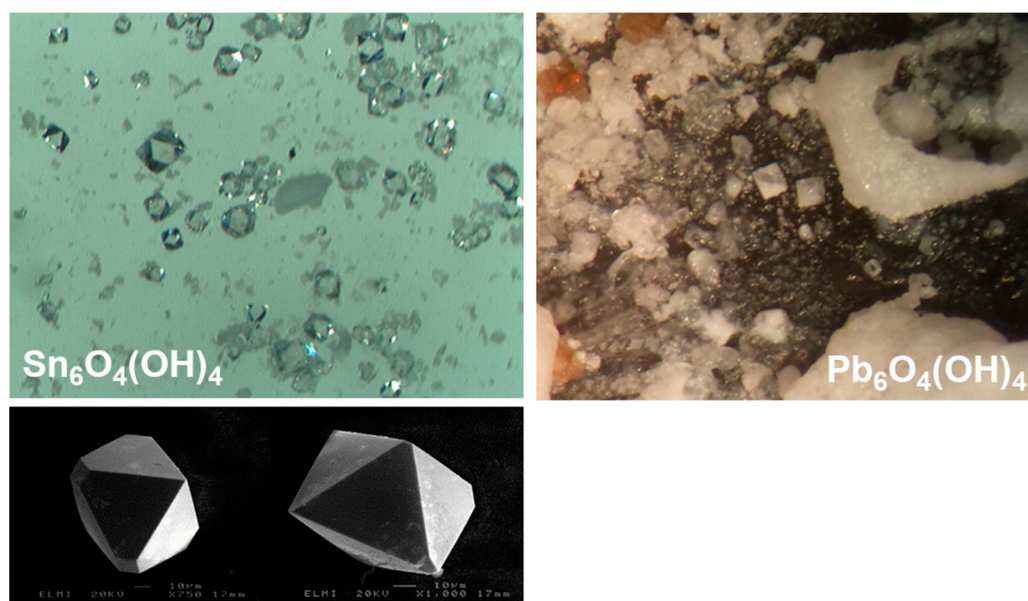


Figure 1. Images from an optical microscope (above row) of the octahedrally shaped single crystals of $\text{Sn}_6\text{O}_4(\text{OH})_4$ (left) and $\text{Pb}_6\text{O}_4(\text{OH})_4$ (right); scanning electron microscopic images (below row) of selected single crystals of $\text{Sn}_6\text{O}_4(\text{OH})_4$ (left).

$\text{Pb}_6\text{O}_4(\text{OH})_4$: Colorless, octahedral single crystals of the lead compound (Figure 1) have been obtained in a microscale experiment searching by optical microscopy for new strontium acetate hydrates using strontium hydroxide octahydrate, $\text{Sr}(\text{OH})_2 \cdot 8\text{H}_2\text{O}$, as strontium, and solution of lead acetate, $\text{Pb}(\text{OAc})_2$, as acetate sources. After addition, the aqueous solution slowly spread over the petri dish, dissolving some strontium hydroxide octahydrate at the same time. After some days, the main product of such experiments consisted of needle-like single crystals of strontium acetate sesquihydrate, $\text{Sr}(\text{OAc})_2 \cdot \frac{1}{2}\text{H}_2\text{O}$. As side products, we found amorphous orange and yellow solids as well as some single crystals of the title compound (Figure 1). Obviously, the dissolution of the strontium hydroxide by the acidic lead acetate solution generates pH values at specific regions of the petri dish that are favorable for the formation and crystallization of $\text{Pb}_6\text{O}_4(\text{OH})_4$. A possible reaction equation summarizing these observations is sketched out in Scheme 2.



Scheme 2. Possible reaction equation for the formation of $\text{Pb}_6\text{O}_4(\text{OH})_4$ from lead(II) acetate, $\text{Pb}(\text{OAc})_2$, and strontium hydroxide octahydrate, $\text{Sr}(\text{OH})_2 \cdot 8\text{H}_2\text{O}$.

2.2. X-ray Structure Determination

High-resolution X-ray diffraction data ($2\Theta_{\text{max}} = 70^\circ$, $\text{MoK}\alpha$) of the tetragonally crystallizing compounds have been collected conventionally at 100(2) K. In both cases, structure solution and refinement have been successfully performed in the non-centrosymmetric space group $P\bar{4}2_1c$ (no. 114 [23]) after taking special care in space group determination due to systematic absences, an aspect that previous investigations failed to notice. Hence, several controversial opinions exist as to whether space group $P4/mnc$ (no. 128 [23]) or $P\bar{4}2_1c$ (no. 114 [23]) is appropriate for the correct description of the structures. Our observations regarding the existence/non-existence of the relevant systematic absence condition are exemplarily discussed in the case of its visibility for $\text{Sn}_6\text{O}_4(\text{OH})_4$ and in the case of its non-visibility as a result of crystal size for $\text{Pb}_6\text{O}_4(\text{OH})_4$.

In both cases, using the default values of the space group determination program (XPREP [29]) yielded hints of a glide plane ($0kl$ only present for $k + l = 2n$) and 2_1 -screw axes ($00l$ only present for $l = 2n$, $0k0$ only present for $k = 2n$, and hhl only present for $h = 2n$)

exclusively present in the tetragonal space groups $P4/mnc$ (No. 128, centrosymmetric) and $P4nc$ (No. 104, non-centrosymmetric) [23].

$\text{Sn}_6\text{O}_4(\text{OH})_4$: In combination with the results of the E-value statistic (mean $|E^*E-1| = 0.912$), structure solution and refinement of the tin compound were first performed in the centrosymmetric space group $P4/mnc$. The resulting structure model consisted of a $\text{Sn}_6\text{O}_4(\text{OH})_4$ molecule of point group symmetry C_{4v} with all eight oxygen atoms related to each other via a fourfold rotation axis perpendicular to a mirror plane. Although the results obtained by using this structure model look quite good [$M = \text{Sn}$: $R1 = 0.0400$ and $wR2 = 0.0841$], there are some aspects like the high rest electron density [$\pm\Delta e = 3.874/-3.319 \text{ e}\text{\AA}^3$, $0.45/-0.10 \text{ \AA}$ apart from O1] and the high anisotropy of the thermal displacement ellipsoid (Figure 2I; for $M = \text{Pb}$, see Figure S1I) of the oxygen atom that are less convincing. In combination with the great number of alerts generated from the structure validation program checkCIF [30,31] and some further critical data like the weighting parameters p and q , all summarized in Table S1 (see additional information in supplementary materials), this structure model appeared improper for the structure description.

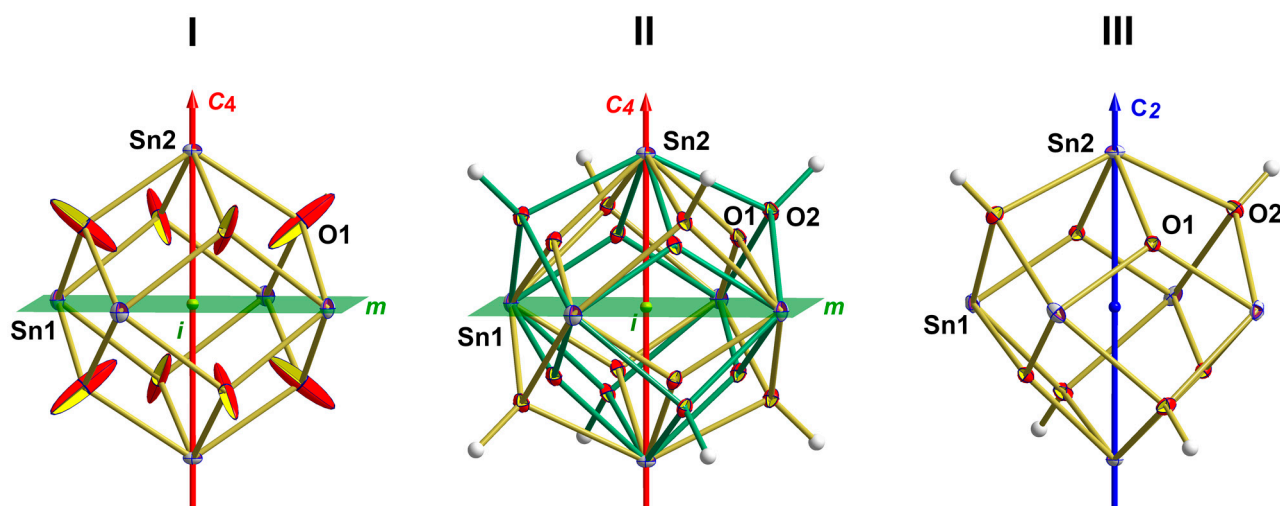


Figure 2. Ball-and-stick models of the $\text{Sn}_6\text{O}_4(\text{OH})_4$ molecule as a result of the different structure models in the two different space groups $P4/mnc$ (I,II) and $P42_1c$ (III); structure models (I,II), point group C_{4h} with mirror planes m (green), center of symmetry i (dark green), and proper rotation axis C_4 (as part of a S_4 rotoinversion axis, red); structure model (III), point group S_4 with a fourfold rotoinversion axis (blue, blue sphere = center of symmetry of the rotoinversion axis).

Implementing disordered oxygen atoms in the refinement [free refinement of site positions and thermal displacement parameters, half-occupancy] improved the structure model significantly [$R1 = 0.022$ and $wR2 = 0.0605$ for $I > 2\sigma(I)$, $\pm\Delta e = 1.71/-1.60 \text{ e}\text{\AA}^3$, $1.96/1.27 \text{ \AA}$ apart from Sn(2), see also Table S1 for more critical data and checkCIF results] and revealed in addition a possible hydrogen atom position associated with one of the two oxygen atoms. In summary, this structure model II (Figure 2II; for $M = \text{Pb}$, see Figure S1II) turned out to be the overlay of two different orientations of two $\text{Sn}_6\text{O}_4(\text{OH})_4$ molecules with a $\mu_3\text{-OH}$ group structurally different from the $\mu_3\text{-O}$ atom.

This structure model was formerly described by Hill [22] for the lead and very recently by Dubrovinskaia et al. [17] for the tin compound. Hill, however, pointed out that—from a chemical point of view—the structure is better refined in space group $P42_1c$ instead of $P4/mnc$ in order to prevent the disorder. Both space groups are related to each other by a group-subgroup relationship [23], with $P42_1c$ affording the absence of the glide plane and the omission of the systematic absence condition $0kl$ only present for $k + l = 2n$ [23]. Unfortunately, Hill provided no crystallographic evidence for this assumption, as do Abrahams et al. [21] in the case of the tin compound.

On this background, it seemed appropriate to check the results of structure model II in more detail. Although very good from the viewpoint of refinement, the data check (SHELXL) in space group $P4/mnc$ indicated a large number (789 before merging) of systematic absence violations, 4 (before merging) resulting from violations of the $00l$ and 20 (before merging) from violations of the hkl condition, but most for the $0kl$ condition of the glide plane. On the first view, these systematic absence violations are less conspicuous as all are very weak [$F_o^2(0kl)_{\max}/F_o^2(hkl)_{\max} \leq 0.118$, $F_o^2(0kl)_{\text{mean}} = 0.052$], their great number in combination with the precession they had been measured [$(F_o^2)_{\text{mean}}/\sigma(F_o^2)_{\text{mean}} = 6.79$], however, let us examine the crystallographic background in more detail.

First, we went back to space group determination in order to inspect the exception from systematic absences in more detail. In reducing the gap between observed and unobserved reflections, the criteria of the glide plane vanished, and space group $P42_1c$ came into sight. Second, we simulated precession photography of the $0kl$ -layers from the raw data sets. For $M = \text{Sn}$, this layer image (Figure 3) revealed that all reflections ($0kl$) with $k + l = \text{uneven}$ are present but considerably weaker than those with $k + l = \text{even}$. In the case of our quite large single crystals, these reflections were measurable with sufficient precision, but when scaling down the size of the crystals ($M = \text{Pb}$), they vanish in the background and become undetectable.

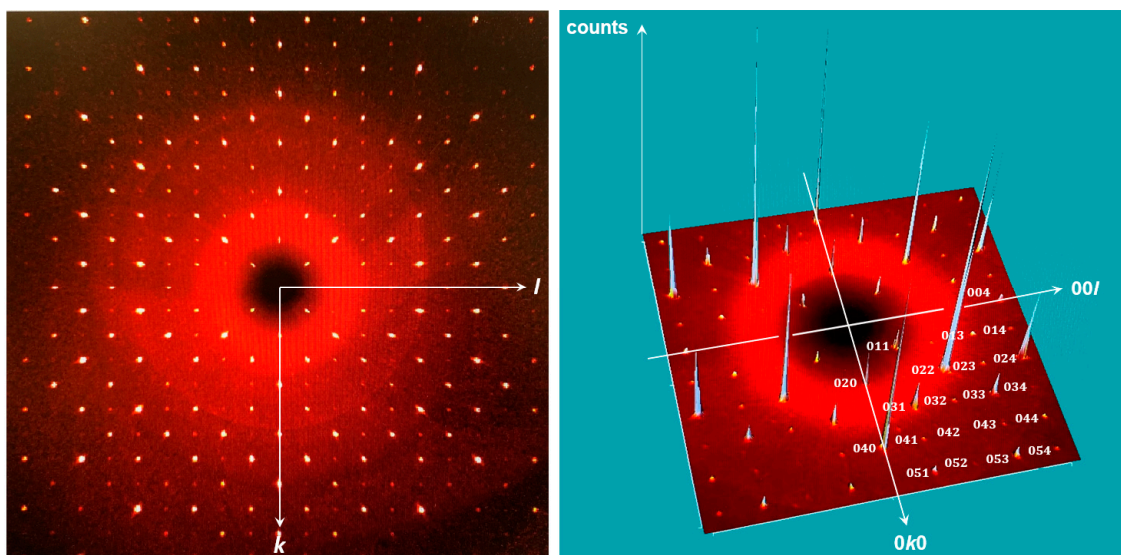


Figure 3. From raw-data simulated precession photography of the $0kl$ -layer of the dataset from $\text{Sn}_6\text{O}_4(\text{OH})_4$, showing the presence of reflections $k + l = 2n + 1$.

$\text{Pb}_6\text{O}_4(\text{OH})_4$: The effect of crystal size on the visibility of the violation of the systematic absence condition $0kl$ with $k + l = 2n$ became apparent when analyzing the data set of the lead compound. The crystal size of the lead compound ($0.020 \times 0.010 \times 0.010$ mm) was about $1/200$ that of the tin compound ($0.075 \times 0.073 \times 0.073$ mm). On the one hand, the smaller crystal size should be partly compensated by the higher scattering power of lead; on the other hand, the smaller crystal size seemed more appropriate with respect to the higher X-ray absorption by the lead compound [$\mu(\text{Sn}_6\text{O}_4(\text{OH})_4)/\mu(\text{Pb}_6\text{O}_4(\text{OH})_4) = 13.133/85.455 \text{ mm}^{-1}$]. In addition, during data collection, we took into account the smaller crystal size by using a longer exposure time [2 s/frame for $M = \text{Sn}$, 5 s/frame for $M = \text{Pb}$].

In the case of reflection (004), the strongest one in both unmerged raw datasets, these different effects give rise to an intensity distribution between $\bar{I}_o(004)_{\text{Sn}}$ and $\bar{I}_o(004)_{\text{Pb}}$ of $49,705/5862 = 8.5:1$, while the precession of these reflections expressed in $\bar{I}_o/\sigma(\bar{I}_o)$ is reduced from 112:1 (Sn) to 45:1 (Pb). Among the reflections of zone $0kl$, reflection (023) shows the highest intensity in the tin dataset, with $\bar{I}_o(023) = 362.8$ and $\sigma(\bar{I}_o) = 8.24$. Assuming that these and the former relationship count throughout the complete data sets of both compounds, one calculates for reflection (023) of the lead compound an I_o -value

of 42.7 with a precession $\sigma(I_o)$ of 3.3, both near the observational limits of our instrument. Actually, the conditions are even poorer, with a $\bar{I}_o(023)_{Pb} = 20.0$ and $\sigma(\bar{I}_o)(023)_{Pb} = 10.9$.

On this background, it is not surprising that in comparison with the tin compound, the number of systematic absence violations is downscaled (46/4, before merging) when solving and refining the lead compound in space group $P4/mnc$ (Table S1). The resulting structure models I and II are presented in Figure S1. Again, structure model II improves the reliability factors and some other validation parameters [$R1 = 0.0147$, $wR2 = 0.0324$ for $I > 2\sigma(I)$, $\pm\Delta e = 1.496/-1.939 \text{ e}\text{\AA}^3$ 1.42/0.70 \AA apart from Pb1] significantly in comparison to structure model I [$R1 = 0.0217$, $wR2 = 0.0421$ for $I > 2\sigma(I)$, $\pm\Delta e = 4.435/-4.070 \text{ e}\text{\AA}^3$ 0.44/0.04 \AA apart from O]. More critical data and the results from checkCIF validation are listed in Table S1.

Even if all the data in structure model II gives the impression that everything is correct, the refinement of the lead compound according to structure model III seemed meaningful. The improvements by this structure model III are less pronounced (Table S1) in view of the values/parameters discussed above for the tin compound, but they reduce the systematic absence violations as a result of the non-existing glide plane and eliminate the disorder of the molecule.

3. Results and Discussion

Our single crystal structure determinations (Table 1) at low temperature (100 K) confirm the previous results [21,22] obtained from powder data at room temperature with respect to the cell parameters of the tetragonal unit cell of space group $P\bar{4}2_1c$. In addition, they indicate the existence of this structure type up to $T = 100 \text{ K}$. In both cases, we examined non-twinned single crystals, but the absolute structure of the lead compound presented here is opposite that of the tin compound (see below).

Table 1. Crystallographic data and results of refinement in the final structure models III.

$M_6O_4(OH)_4$	M = Sn	M = Pb
Empirical formula	$H_4O_8Sn_6$	$H_4O_8Pb_6$
Formula weight [g/mol]	844.17	1375.17
Temperature [K]		100(2)
Crystal system		tetragonal
Space group	$P\bar{4}2_1c$	
a [\AA]	7.8788(1)	7.9693(3)
c [\AA]	9.0582(1)	9.2741(3)
Volume [\AA^3]	562.29(3)	589.00(5)
Z, Z', d_{calc} [g/cm^3]	2, 1, 4.986	2, 1, 7.754
μ ($\text{MoK}\alpha$) [mm^{-1}]	13.133	85.455
F(000)	736	1120
$2\Theta_{\text{max}}$		70°
Reflections collected	53,360	116,076
Reflections unique, R_{int}	1242/0.0600	1304/0.0999
Data/restraints/parameters	21,242/0/35	1304/0/35
Goodness-of-fit on F^2	1.332	1.106
R1/wR2 [$I > 2\sigma(I)$]	0.0127, 0.0277	0.0157, 0.0285
R1/wR2 [all data]	0.0133, 0.0278	0.0197, 0.0293
Extinction coefficient	0.00271(19)	0.00121(5)
Absolute structure parameter	-0.01(2)	0.021(15)
$\pm\Delta e$ [$\text{e}\text{\AA}^{-3}$]	0.553/-0.552	1.135/-1.880

3.1. Overall Structure of the $M_6O_4(OH)_4$ Molecules

Because of space group symmetry, the asymmetric unit consists of one quarter of the formula with one metal atom [M2] on a fourfold rotoinversion axis and one metal atom [M1], one oxygen atom [O2], and one hydroxyl group [O1], all in general position (Figure 4). In summary, both molecules belong to point group symmetry S_4 .

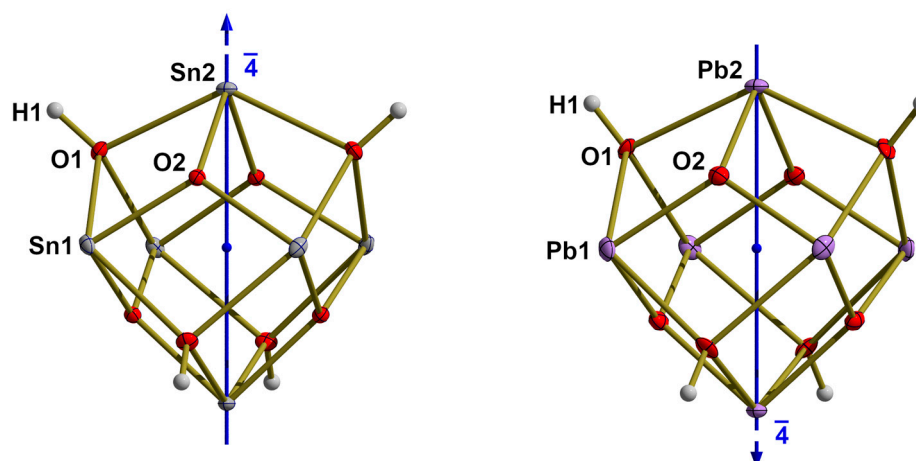


Figure 4. Ball-and-stick model of the $M_6O_4(OH)_4$ molecules with labeling of the asymmetric units; their orientation with respect to the crystallographic c -axis (=absolute structure) is indicated by the blue arrow at the top of the fourfold rotoinversion axes (blue sphere = inversion center of $\bar{4}$).

The six metal atoms of the $M_6O_4(OH)_4$ molecules are arranged at the corners of octahedra that are slightly distorted. First, the four metal M1-atoms are not coplanar but $\pm 0.0020(2)/\pm 0.0032(2)$ Å ($M = \text{Sn}/\text{Pb}$) apart from their least-squares planes that are perpendicular to the fourfold rotoinversion axes through the M2-atoms. Second, and more instructive for the structural differences between the tin and lead compounds, the $\{M_6\}$ -octahedra are elongated/compressed in the direction of the c -axis. Designating $d(\text{Sn}2 \cdots \text{Sn}2)$ as d_{ax} and the distance $d(\text{Sn}1 \cdots \text{Sn}1)$ between two adjacent metal atoms in idealized octahedral positions ($z_M = 0$) as d_{eq} , the elongation in the case of $M = \text{Sn}$ is expressed by $d_{ax}/d_{eq} = 5.0145(1)/5.0082(1)$ Å, $\Delta = 0.0063$ Å and the compression in the case of $M = \text{Pb}$ by $d_{ax}/d_{eq} = 5.1698(3)/5.2339(3)$ Å, $\Delta = -0.0641$ Å.

All faces of the $\{M_6\}$ -octahedra are capped by oxygen atoms alternating between $\mu_3\text{-O}$ and $\mu_3\text{-OH}$ types. The resulting $\{O_4\}$ -tetrahedra are significantly larger for the $\mu_3\text{-OH}$ atoms [O2] than those of the $\mu_3\text{-O}$ atoms [O1]. In both cases, the fourfold rotoinversion axes cross two opposite $\text{O} \cdots \text{O}$ edges. Labeling the edge to opposite edge distances in direction of the c -axis with d_1 and those in the ab -plane with d_2 , the tetrahedra of the $\mu_3\text{-OH}$ atoms are elongated for $M = \text{Sn}$ [$d_1/d_2 = 3.011(2)/3.045(2)$] and compressed for $M = \text{Pb}$ [$d_1/d_2 = 3.172(6)/3.142(6)$ Å] while for the tetrahedra of the $\mu_3\text{-O}$ atoms the proportions go into reverse: for $M = \text{Sn}$ [$d_1/d_2 = 2.226(2)/2.190(2)$ Å] the tetrahedron is compressed and for $M = \text{Pb}$ [$d_1/d_2 = 2.308(6)/2.371(6)$ Å] it is elongated. All in all, the three polyhedra are arranged in the form of a stella octangula (Figure 5).

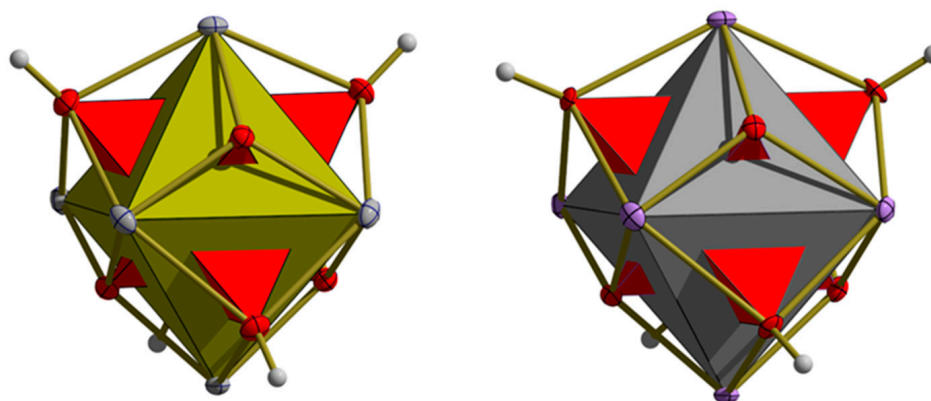


Figure 5. Stella octangula resulting from the interpenetration of the two different oxygen tetrahedra (red) with the octahedron of the tin (messing, left) and lead (dark grey, right) atom octahedra.

Taking the van-der-Waals radii into account, the molecules exhibit an almost spherical shape (Figure 6), with diameters around 0.948/0.956 nm ($M = \text{Sn}/\text{Pb}$). Since there are two $M_6O_4(\text{OH})_4$ molecules per unit cell, their effective mol volume calculates to 281.15 \AA^3 for $M = \text{Sn}$ and 294.50 \AA^3 for $M = \text{Pb}$.

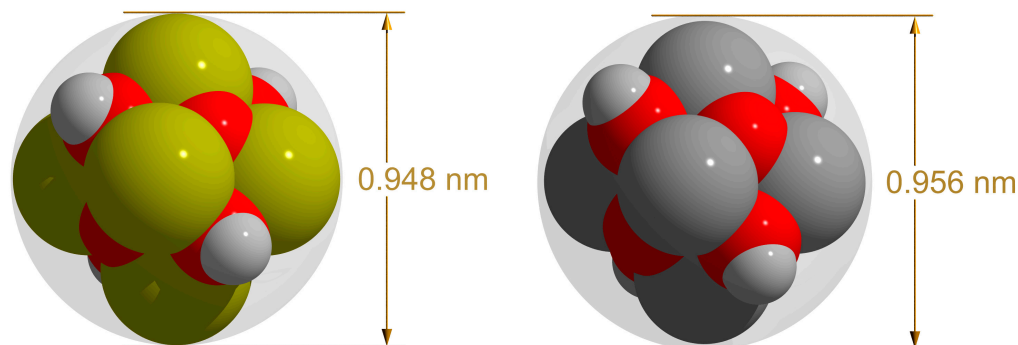


Figure 6. Space-filling model of the $\text{Sn}_6\text{O}_4(\text{OH})_4$ (left) and $\text{Pb}_6\text{O}_4(\text{OH})_4$ (right) molecule with enclosing sphere, color code, and van-der-Waals radii used [32]: oxygen = red, 1.52 \AA ; hydrogen = grey, 0.95 \AA ; tin = bronze, 2.11 \AA ; lead = dark grey, 2.05 \AA .

3.2. Metal-Atom Coordination Polyhedra

Both crystallographic independent metal atoms are fourfold, seesaw (ss) coordinated with two μ_3 -oxygen atoms [O2] in *equatorial* and two μ_3 -hydroxyl groups [O1] in *axial* positions (Figures 7 and 8 for $M = \text{Sn}$; Figures S3 and S4 for $M = \text{Pb}$). Although these $\{\text{MO}_4\}$ -coordination polyhedra only exhibit C_1 [M1] and C_2 point group symmetry [M2]—the twofold rotation axis is part of the crystallographic, fourfold rotoinversion axis—their bond lengths and angles only differ marginally from those for an ideal *bent* seesaw coordination of point group symmetry C_{2v} . Therefore, they can be thought of as prototypes for the $\{\text{MO}_4\}_{\text{ss}}$ -coordination of bivalent tin and lead.

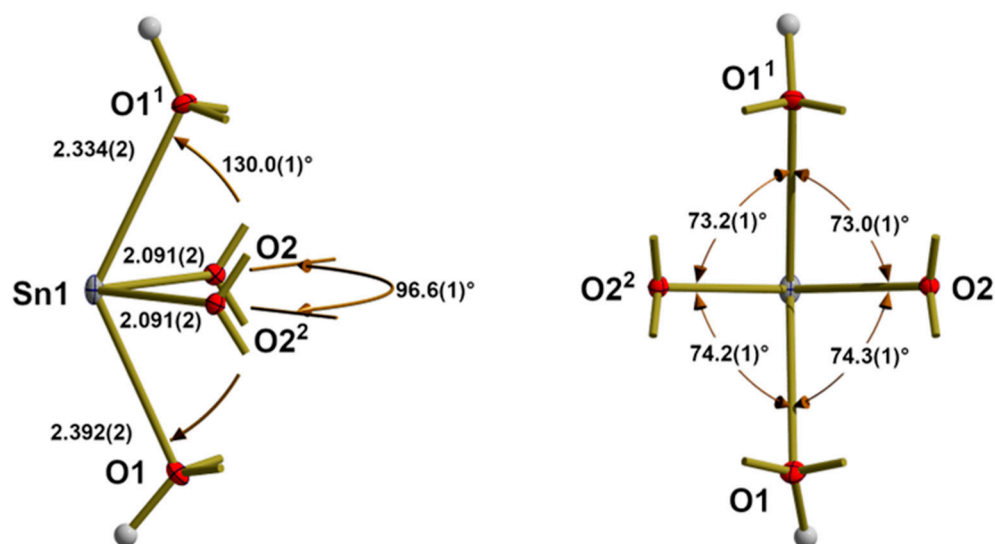


Figure 7. Different views [left side = side view, right side = from bottom up] on the ball-and-stick model of the bended seesaw $\{\text{SnO}_4\}$ coordination of Sn1 with bond lengths [Å] and angles [$^\circ$]; additional bonds of the oxygen atoms are indicated as shortened sticks; symmetry operations used to generate equivalent atoms: $(^1) -y, x, -z$; $(^2) y, -x, -z$.

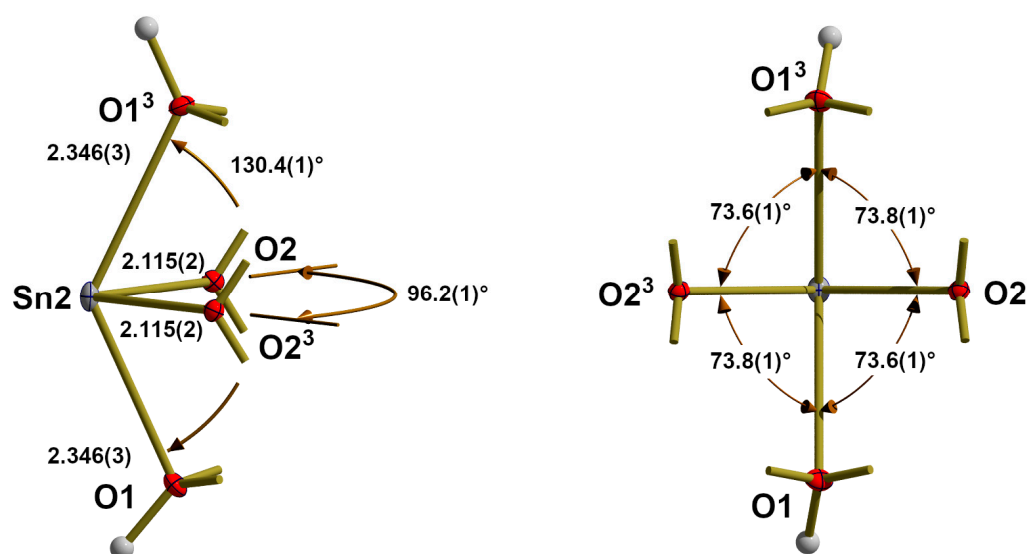


Figure 8. Different views [left side = side view, right side = from bottom up] on the ball-and-stick model of the bended seesaw $\{SnO_4\}$ coordination of Sn2 with bond lengths [Å] and angles [°]; additional bonds of the oxygen atoms are indicated as shortened sticks; symmetry operations used to generate equivalent atoms: $(^3) -x, -y, z$.

Bond lengths between the central metal atom and the equatorial oxygen atoms are 2.091(2)/2.091(2) Å [equal by chance] for Sn1 and 2.115(2) Å for Sn2. The corresponding values for the lead compound are 2.184(5)/2.192(5) Å for Pb1 and 2.204(5) Å for Pb2. As expected, these bond lengths are significantly shorter than those to the axial oxygen atoms, where values of 2.334(2) and 2.392(2)/2.346(3) Å for Sn1/Sn2, and 2.456(6) and 2.475(5)/2.436(5) Å for Pb1/Pb2 are observed. Differences between *axial* and *equatorial* bond lengths, BL , are of the same magnitude for both tin and lead, with somewhat larger absolute values for M1 [$\Delta_{\text{mean}}(BL_{\text{ax}}-BL_{\text{eq}}) = 0.231/0.232$ Å for $M = Sn/Pb$] in comparison with those for M2 [$\Delta(BL_{\text{ax}}-BL_{\text{eq}}) = 0.272/0.278$ Å for $M = Sn/Pb$].

Comparing the bond lengths of tin and lead in the $M_6O_4(OH)_4$ molecules, the latter are 0.089/0.097 Å [$\Delta_{\text{mean}}BL_{\text{ax}}/\Delta BL_{\text{eq}}$] longer than those in the tin molecule. These values are of the same magnitude as the differences between the atom radii of tin and lead calculated from SCF functions [33].

From the different parameters for bond valence calculations, BVS, available in literature [34–38], those of Sidey [38] for Sn–O [$R_0 = 1.849$, $B = 0.5$] and Krivovichev and Brown [37] for Pb–O [$R_0 = 1.963$, $B = 0.49$] give the best agreement with the oxidation state of +II for the metal atoms: $BVS_{Sn1} = 1.99$, $BVS_{Sn2} = 1.92$; $BVS_{Pb1} = 1.98$, $BVS_{Pb2} = 1.98$.

Despite the larger size of lead in comparison to tin, most bond angles are very similar in both compounds, with the exception of the equatorial bond angles [$96.6(1)^\circ/96.2(1)^\circ$ for Sn1/Sn2, $98.3(3)^\circ/99.1(3)^\circ$ for Pb1/Pb2] that are considerably larger for $M = Pb$. A simple but appropriate bonding concept for a $\{M^{II}X_4\}_{\text{ss}}$ coordination, taking into account the observed acute bond angles and the non-bonding electron pair of a bivalent group-14 element, has previously been described for $M = Sn$ [39].

3.3. Oxygen Atom Coordination

Both oxygen atoms of the asymmetric unit are trigonal-pyramidally coordinated with the oxygen atom at the top of the pyramid (Figure 9 for $M = Sn$, Figure S4 for $M = Pb$). Differences in bond lengths, bond angles, and height of the trigonal pyramid result from the fact that O1 belongs to a μ_3 -hydroxyl group while O2 constitutes a μ_3 -oxo group. Moreover, both oxygen atoms are involved in hydrogen bonds, with O1 as the donor and O2 as the acceptor.

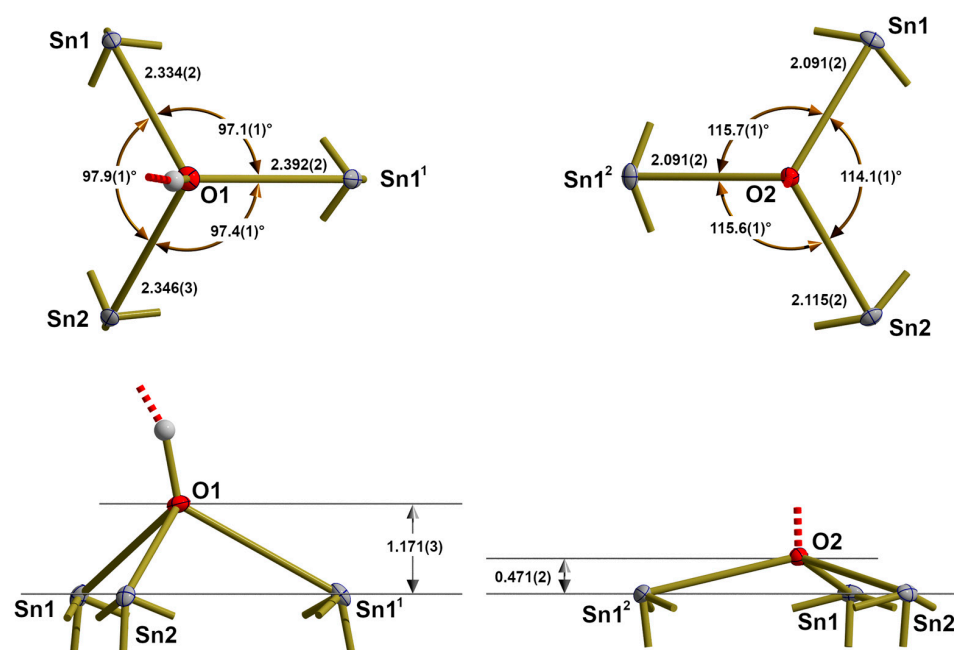


Figure 9. Different views [above = from top, below = side view] on the ball-and-stick models of the trigonal-pyramidal coordination of O1 (left) and O2 (right) with bond lengths [Å] and angles [°]; additional bonds of the oxygen atoms are indicated as shortened sticks; symmetry operations used to generate equivalent atoms: ⁽¹⁾ $y, -x, -z$; ⁽²⁾ $-y, x, -z$.

In the trigonal pyramid of μ_3 -O1 the metal to oxygen distances range from 2.334(2)–2.346(3) Å, mean value = 2.357(25) Å for M = Sn, and from 2.356(6)–2.367(7) Å, mean value = 2.456(16) Å for M = Pb, while bond angles range from 97.08(3)°–97.15(3)° [mean value = 97.5(4)°] for M = Sn and 97.2(2)°–97.3(2)° [mean value = 97.3(1)°] for M = Pb. With these structural parameters, the oxygen atoms are 1.171(3) Å [M = Sn] and 1.226(6) Å [M = Pb] above the basal plane of the three metal atoms. With respect to the fact that O1 is also bonded to a hydrogen atom, the bond angles are indicative that it is sp^3 hybridized.

In contrast, the trigonal pyramids of μ_3 -O2 are more flattened, with oxygen atoms 0.471(2) Å [M = Sn] and 0.531(6) Å [M = Pb] above the basal plane of the metal atoms. With bond lengths [range: 2.091(2)–2.115(2) Å, mean value: 2.099(11) Å, M = Sn; range: 2.184(5)–2.204(5), mean value: 2.193(8) Å, M = Pb] and angles [range: 114.1(1)°–115.7(1)°, mean value = 115.7(7)°, M = Sn/range: 113.5(2)°–115.5(2)°, mean value: 114.3(8)°, M = Pb], these oxygen atoms reflect sp^2 -hybridization.

3.4. Hydrogen Bonding

Hydrogen atoms of the μ_3 -OH groups could be localized from difference Fourier synthesis. For M = Pb, its position correlates approximately with the position of the hydrogen atom determined by Hill [22] from neutron powder data. For M = Sn, the hydrogen position has never been described before. In both cases, the hydroxyl groups act as donors in hydrogen bonds to μ_3 -O atoms of neighboring molecules as acceptors. Bond lengths and angles are summarized in Table 2.

Table 2. Geometry of the hydrogen bonds [Å, °] in the crystal structures of $\text{Sn}_6\text{O}_4(\text{OH})_4$ and $\text{Pb}_6\text{O}_4(\text{OH})_4$.

	d(D-H)	d(H...A)	d(D...A)	<(D-H...A)
M = Sn ¹	0.96	1.96(0)	2.881(4)	160.4(0)
M = Pb ²	0.96	1.91(0)	2.819(9)	156.3(0)

Symmetry transformations used for the generation of equivalent atoms: ⁽¹⁾ $x+1/2, -y+1/2, -z+1$; ⁽²⁾ $-x+1/2, y-1/2, -z+1/2$.

3.5. Packing

In the solid, the molecules are linked via eight hydrogen bonds with eight others, cube-like arranged ones (Figure 10).

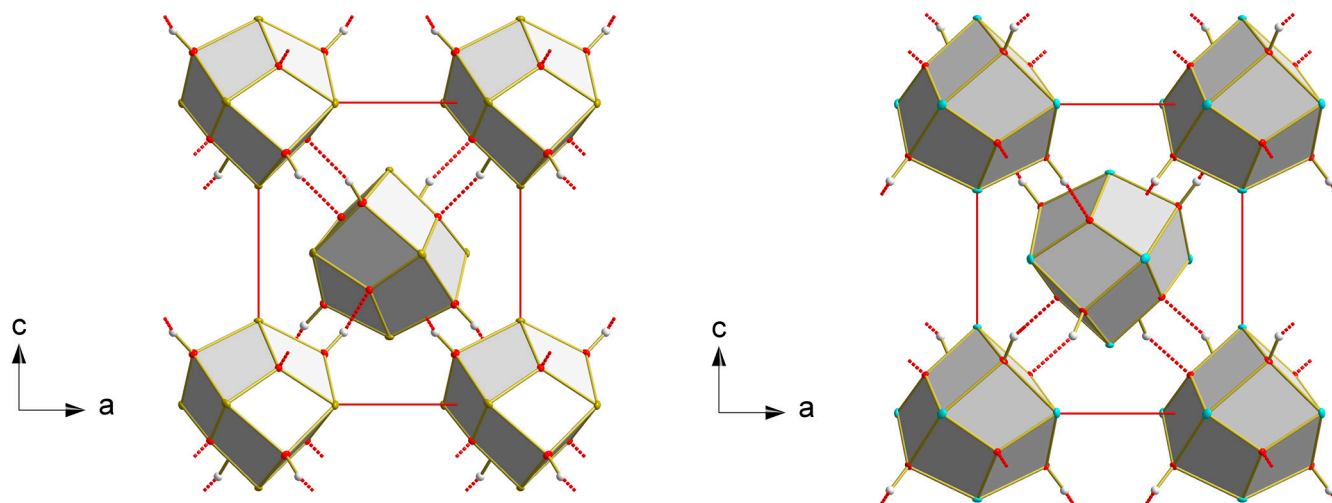


Figure 10. Packing of the $\text{Sn}_6\text{O}_4(\text{OH})_4$ (left) and $\text{Pb}_6\text{O}_4(\text{OH})_4$ (right) molecules looking down the b-axis. The different absolute structures of both can be recognized when looking at the central molecules, inspecting their faces, and analyzing their hydrogen bonds.

3.6. Related Compounds

The structures of many other tin(II) and lead(II) compounds are related to the metal-oxygen backbone of the $\text{M}_6\text{O}_4(\text{OH})_4$ molecules. First of all, tin(II) alkoxides, $\text{Sn}(\text{OR})_2$, lead(II) alkoxides, and $\text{Pb}(\text{OR})_2$, partially hydrolyze to compounds with the formula $\text{M}_6\text{O}_4(\text{OR})_4$, where alkoxide ligands substitute the OH groups of the title compounds. Typical structures with, e.g., pure carbon hydrogen ligands are described for $\text{M} = \text{Sn}$ and $\text{R} = \text{Me}$ [40], Et [41,42], $t\text{Bu}$ [43], Neopentyl [44], $i\text{Pr}$ -Phenyl [45], and for $\text{M} = \text{Pb}$ and $\text{R} = i\text{Pr}$ [46,47]. In addition, two pure inorganic, anthropogenic tin derivatives have been structurally characterized [48]: the cation $[\text{Sn}_6\text{O}_4(\text{OH})_2]^{2+}$ with two missing hydroxyl groups in compound $[\text{Sn}_6\text{O}_4(\text{OH})_2][\text{SO}_4]$ and the cation $[\text{Sn}_6\text{O}_4]^{4+}$ where each hydroxyl group of the parent compound $\text{Sn}_6\text{O}_4(\text{OH})_6$ is replaced by one oxygen atom of a $\{\text{SiO}_4\}$ tetrahedron in the compound $[\text{Sn}_6\text{O}_4][\text{SiO}_4]$.

4. Conclusions

The crystal structure determinations of the title compounds show that (i) in some unfavorable circumstances (here: small intensities of the relevant reflections in combination with small crystals), a given dataset may pretend a systematic absence condition that in reality does not exist, and (ii) that a well-resolved dataset, even if the reflections in question are absent (here: because they are too small, omitted, or undetected), may deliver enough structural information from the remaining reflections for a top-quality structure refinement. Moreover, our calculations of the different structure models demonstrate that structure refinement in the pretended, higher-symmetrical space group may result in plausible structure models. Some unusual parameters, most often recognized and mentioned by refinement or structure validation programs, are, however, indicators that something may be wrong. Trying to circumvent some of these problems by using disordered structure models may improve the structure model to an excellent state but will not solve the actual space group problem resulting from the pretended systematic absence condition. Only structure refinement in the correct, lower symmetrical space group—sometimes only obtainable when taking group-subgroup relationships into account—will improve the reliability of the well-ordered structure model significantly and will eliminate all relevant validation alerts.

5. Experimental Details

5.1. Preparation

5.1.1. $\text{Sn}_6\text{O}_4\text{OH}_4$

Single crystals have been found during disposal of some decades-old solutions of various monoorganotin(IV) trihydrides (RSnH_3 with $\text{R} = \text{Et}, {}^n\text{Pr}, {}^i\text{Pr}, {}^n\text{Bu}, {}^i\text{Bu}$) in mixtures of toluene and *N,N*-dimethylformamide, DMF. The *trihydrides* have been prepared at 0°C via the reduction of monoorganotin(IV) chlorides, RSnCl_3 , dissolved in toluene with commercially available 1M solutions of lithium tetrahydridoaluminate, $\text{Li}[\text{AlH}_4]$, in diethylether (molar ratio 1:4). After completion of the reaction, the solution was warmed up to room temperature and stirred for an additional 2 h before the reaction mixture was worked up with a water-ice mixture. The organic layer was subsequently separated and dried with anhydrous sodium sulfate before dry DMF was added. Thereafter, the clear solutions turned red very quickly before they were stored in carefully sealed flasks. All steps have been performed in an inert atmosphere of N_2 and Ar, respectively. After more than a decade of storage, well-shaped, colorless single crystals of the title compound were found at the bottom of most of the flasks. The samples retained their color over the entire time of storage, but when coming into contact with air after opening, the color disappeared quickly.

Monoorganotin(IV) trichlorides, RSnCl_3 , have been prepared according to procedures described in the literature ($\text{R} = {}^i\text{Pr}, {}^n\text{Pr}$ [49], ${}^i\text{Bu}$ [50]) or have been obtained commercially ($\text{R} = \text{Et}, {}^n\text{Bu}$).

5.1.2. $\text{Pb}_6\text{O}_4(\text{OH})_4$

In the middle of a small ring formed on a petri dish from solid $\text{Sr}(\text{OH})_2 \cdot 8\text{H}_2\text{O}$, about 10 mL of a 1.38M solution of $\text{Pb}(\text{OAc})_2$ are added dropwise. The following processes were monitored using an optical microscope (Stemi 1000, Zeiss, Oberkochen, Germany). When the solution reached and penetrated the solid, the strontium compound started to dissolve in part, and color changes indicated the beginning of some reactions. After some days, large amounts of colorless, needlelike single crystals of $\text{Sr}(\text{OAc})_2 \cdot \frac{1}{2}\text{H}_2\text{O}$ have been found at the position where the hydroxide originally was placed. In addition, a few single crystals of the title compound have been detected in between, as have a few amorphous, yellow, and red solids of unknown (PbO and Pb_3O_4) composition.

5.2. Single Crystal X-ray Structure Determination

Single crystals suitable for X-ray measurements were selected under a microscope and mounted on a 50 μm MicroMesh MiTeGen MicromountTM (MiTeGen, Ithaca, NY, USA) using FROMBLIN Y perfluoropolyether (LVAC 16/6, Aldrich, St. Louis, MO, USA) before they were centered on a Bruker Kappa APEX II CCD-based 4-circle X-ray diffractometer using graphite monochromated Mo $\text{K}\alpha$ radiation ($\lambda = 0.71073 \text{ \AA}$) of a fine focus molybdenum-target X-ray tube operating at 50 kV and 30 mA. The crystal-to-detector distance was 40 mm, and exposure time was 2/5 s per frame for $\text{M} = \text{Sn}/\text{Pb}$ with a scan width of 0.5° . Samples were cooled stepwise to 100 K by using a Kryoflex low-temperature device. No structural changes have been detected during cooling.

Data were integrated and scaled using the programs SAINT and SADABS [51] within the APEX2 software package of Bruker [29]. Special care was taken regarding the data collection strategy in order to reduce absorption effects. A maximum reduction of absorption effects and remaining electron density was achieved by high data redundancies ($\text{Sn}/\text{Pb} \approx 43/89$, mean values) and empirical absorption corrections.

Structures were solved by direct methods with SHELXS [52] and completed by difference Fourier synthesis with SHELXL [52]. Structure refinements were carried out on F^2 using full-matrix least-squares procedures, applying anisotropic thermal displacement parameters for all non-hydrogen atoms. H atoms have been clearly identified in difference-Fourier syntheses. They were refined with an O-H distance of 0.96 Å before they were fixed and allowed to ride on the corresponding oxygen atom with an isotropic temperature factor.

Details on the crystallographic data, data collection parameters, and results of structure refinement are summarized in Table 1 with $R_{\text{int}} = \Sigma |F_o^2 - F_o^2(\text{mean})| / \Sigma [F_o^2]$ and $R_\sigma = \Sigma [\sigma(F_o^2)] / \Sigma [F_o^2]$. Final agreement indices: $R_1 = \Sigma ||F_o| - |F_c|| / \Sigma |F_o|$ and $wR_2 = [\Sigma [w(F_o^2 - F_c^2)^2] / \Sigma (F_o^2)^2]^{1/2}$. Weighting function used: $w = 1 / [\sigma^2(F_o^2) + (pP)^2 + qP]$ with $P = (F_o^2 + 2F_c^2) / 3$. $\text{Goof} = [\Sigma [w(F_o^2 - F_c^2)^2] / (n - p)]^{1/2}$, where n is the number of reflections and p is the total number of parameters refined.

Figures have been drafted using Diamond [53] and realized by POV-Ray [54]. Without the hydrogen atoms that are drawn as spheres of arbitrary radius, all other atoms are drawn as thermal displacement ellipsoids of the 50% level.

Supplementary Materials: The following supporting information can be downloaded at: <https://www.mdpi.com/article/10.3390/cryst13050739/s1>, Figure S1: Ball-and-stick models of $\text{Pb}_6\text{O}_4(\text{OH})_4$ as result of the different structure models in the two different space groups $P4/mnc$ (I, II) and $\bar{P}42_1c$ (III); structure model I and II, point group C_{4h} with mirror planes m (green), center of symmetry i (dark green) and proper rotation axis C_4 (as part of a S_4 rotoinversion axis, red); structure model III, point group S_4 with S_4 rotoinversion axis (blue, blue sphere = center of symmetry of the rotoinversion axis); Table S1: Summary of the effect of the different space groups and structure models on some dataset, refinement and validation parameters for $\text{Sn}_6\text{O}_4(\text{OH})_4$ and $\text{Pb}_6\text{O}_4(\text{OH})_4$; Table S2: Full list of bond lengths [Å] and angles [°] for $\text{Sn}_6\text{O}_4(\text{OH})_4$; Table S3: Full list of bond lengths [Å] and angles [°] for $\text{Pb}_6\text{O}_4(\text{OH})_4$; Table S4: Atomic coordinates ($\times 10^4$) and equivalent isotropic/anisotropic displacement parameters ($\text{Å}^2 \times 10^3$) for $\text{Sn}_6\text{O}_4(\text{OH})_4$. The anisotropic displacement factor exponent takes the form: $-2\pi^2 [h^2a^2U_{11} + \dots + 2hka^*b^*U_{12}]$. $U(\text{eq})$ is defined as one third of the trace of the orthogonalized U_{ij} tensor; Table S5: Atomic coordinates ($\times 10^4$) and equivalent isotropic/anisotropic displacement parameters ($\text{Å}^2 \times 10^3$) for $\text{Pb}_6\text{O}_4(\text{OH})_4$. The anisotropic displacement factor exponent takes the form: $-2\pi^2 [h^2a^2U_{11} + \dots + 2hka^*b^*U_{12}]$. $U(\text{eq})$ is defined as one third of the trace of the orthogonalized U_{ij} tensor; Table S6: Selected bond lengths [Å] and angles for $\text{M}_6\text{O}_4(\text{OH})_4$ with $\text{M} = \text{Sn}, \text{Pb}$; Figure S2: Different views [left side = side view, right side = from bottom up] on the ball-and-stick model of the bended seesaw $\{\text{PbO}_4\}$ coordination of Pb1 with bond lengths [Å] and angles [°]; additional bonds of the oxygen atoms are indicated as shortened sticks; symmetry operations used to generate equivalent atoms: $(^1) 1-y, x, 1-z$; Figure S3: Different views [left side = side view, right side = from bottom up] on the ball-and-stick model of the bended seesaw $\{\text{PbO}_4\}$ coordination of Pb2 with bond lengths [Å] and angles [°]; additional bonds of the oxygen atoms are indicated as shortened sticks; symmetry operations used to generate equivalent atoms: $(^1) 1-y, x, 1-z$; $(^2) y, 1-x, 1-z$; $(^3) 1-x, 1-y, z$; Figure S4: Different views [left side = side view, right side = from bottom up] on the ball-and-stick model of the bended seesaw $\{\text{PbO}_4\}$ coordination of Pb2 with bond lengths [Å] and angles [°]; additional bonds of the oxygen atoms are indicated as shortened sticks; symmetry operations used to generate equivalent atoms: $(^1) 1-y, x, 1-z$; $(^2) y, 1-x, 1-z$; $(^3) 1-x, 1-y, z$. The supplementary material include reports of checkCIF and tables for structure models I and II, tables of bond lengths and angles, atomic coordinates, thermal displacement parameters for structure models III and figures of the lead and oxygen environment in $\text{Pb}_6\text{O}_4(\text{OH})_4$.

Author Contributions: Conceptualization, methodology, X-ray crystallography, visualization, original draft, funding acquisition, H.R.; synthesis, D.S. and K.P. All authors have read and agreed to the published version of the manuscript.

Funding: H.R. and D.S. gratefully acknowledge the Deutsche Forschungsgemeinschaft (DFG) for funding project 5168536 "Synthese polyedrischer Organozinnverbindungen durch Wasserstoffabspaltung aus Hydriden sowie Charakterisierung der Strukturen und Bindungsverhältnisse" in SPP446: Aufbau und Funktionalisierung von Polyeder-Gerüsten aus Hauptgruppenelementen.

Data Availability Statement: Further details of the crystal structure investigations may be obtained from the joint CCDC/FIZ Karlsruhe online deposition service: www.ccdc.cam.ac.uk/structures (accessed on 31 March 2023) by quoting the deposition numbers CSD-2252473 for $\text{Sn}_6\text{O}_4(\text{OH})_4$, and CSD-2252349 for $\text{Pb}_6\text{O}_4(\text{OH})_4$.

Acknowledgments: The authors thank Wilfried Assenmacher, University of Bonn, for the scanning electron microscopic images of the $\text{Sn}_6\text{O}_4(\text{OH})_4$ crystals. The author thanks the Deutsche Forschungsgemeinschaft (DFG) and the Government of Lower Saxony for funding the diffractometer.

Conflicts of Interest: The authors declare no conflict of interest.

References

1. Séby, F.; Potin-Gautier, M.; Giffaut, E.; Donard, O.F.X. A critical review of thermodynamic data for inorganic tin species. *Geochim. Cosmochim. Acta* **2001**, *18*, 3041–3053. [[CrossRef](#)]
2. Perera, W.N.; Hefter, G.; Sipos, P.M. An Investigation of the Lead(II)-Hydroxide System. *Inorg. Chem.* **2001**, *40*, 3974–3978. [[CrossRef](#)] [[PubMed](#)]
3. Hennings, E.; Schmidt, H.; Köhler, M.; Vogt, W. Crystal structure of tin(II) perchlorate trihydrate. *Acta Cryst.* **2014**, *E70*, 474–476. [[CrossRef](#)] [[PubMed](#)]
4. Donaldson, J.D.; Grimes, S.M.; Johnston, S.R.; Abrahams, I. Characterisation of the Tin(II) Hydroxide Cation $[\text{Sn}_3(\text{OH})_4]^{2+}$, and the Crystal Structure of Tritin(II) Tetrahydroxide Dinitrate. *J. Chem. Soc. Dalton Trans.* **1995**, 2273–2276. [[CrossRef](#)]
5. von Schnering, H.G.; Nesper, R.; Pelshenke, H. Hydroxoverbindungen. 10. Über die Natriumoxohydroxostannate(II) $\text{Na}_4[\text{Sn}_4\text{O}(\text{OH})_{10}]$ und $\text{Na}_2[\text{Sn}_2\text{O}(\text{OH})_4]$. *Z. Anorg. Allg. Chem.* **1983**, *499*, 117–129. [[CrossRef](#)]
6. Persson, I.; Lyczko, K.; Lundberg, D.; Eriksson, L.; Placzek, A. Coordination Chemistry Study of Hydrated and Solvated Lead(II) Ions in Solution and Solid State. *Inorg. Chem.* **2011**, *50*, 1058–1072. [[CrossRef](#)]
7. Hong, S.H.; Olin, Å. The Crystal Structure of $[\text{Pb}_4(\text{OH})_4][\text{ClO}_4]_4 \cdot 2\text{H}_2\text{O}$. *Acta Chem. Scand.* **1974**, *28A*, 233–238. [[CrossRef](#)]
8. Grimes, S.M.; Johnston, S.R.; Abrahams, I. Characterisation of the Predominant Low-pH Lead(II)-Hydroxo Cation $[\text{Pb}_4(\text{OH})_4]^{4+}$; Crystal Structure of $[\text{Pb}_4(\text{OH})_4][\text{NO}_3]_4$ and the Implications of Basic Salt Formation on the Transport of Lead in the Aqueous Environment. *J. Chem. Soc. Dalton Trans.* **1995**, 2081–2086. [[CrossRef](#)]
9. Hong, S.-H.; Olin, Å. On the Crystal Structure of $[\text{Pb}_4(\text{OH})_4]_3[\text{CO}_3][\text{ClO}_4]_{10} \cdot 6\text{H}_2\text{O}$. *Acta Chem. Scand.* **1973**, *27*, 2309–2320. [[CrossRef](#)]
10. Kampf, A.R.; Hughes, J.M.; Nash, B.P.; Marty, J. Nitroplumbite, $[\text{Pb}_4(\text{OH})_4](\text{NO}_3)_4$, a New Mineral with Cubane-Like $[\text{Pb}_4(\text{OH})_4]^{4+}$ Clusters from the Burro Mine, San Miguel County, Colorado, USA. *Can. Mineral.* **2022**, *60*, 787–795. [[CrossRef](#)]
11. Kong, F.; Hu, C.-L.; Liang, M.-L.; Mao, J.-G. $\text{Pb}_4(\text{OH})_4(\text{BrO}_3)_3(\text{NO}_3)$: An Example of SHG Crystal in Metal Bromates Containing π -Conjugated Planar Triangle. *Inorg. Chem.* **2016**, *55*, 948–955. [[CrossRef](#)]
12. Spiro, T.G.; Templeton, D.H.; Zalkin, A. The Crystal Structure of a Hexanuclear Basic Lead(II) Perchlorate Hydrate: $\text{Pb}_6\text{O}(\text{OH})_6(\text{ClO}_4)_4 \cdot \text{H}_2\text{O}$. *Inorg. Chem.* **1969**, *8*, 856–861. [[CrossRef](#)]
13. Olin, Å.; Söderquist, R. The Crystal Structure of β - $[\text{Pb}_6\text{O}(\text{OH})_6](\text{ClO}_4)_4 \cdot \text{H}_2\text{O}$. *Acta Chem. Scand.* **1972**, *26*, 3505–3514. [[CrossRef](#)]
14. Organ, R.M.; Mandarino, J.A. Romarchite and hydromarchite, two novel stannous minerals (Abstract). *Can. Mineral.* **1971**, *10*, 916.
15. Ramik, R.A.; Organ, R.M.; Mandarino, J.A. On the type romarchite and hydromarchite from Boundary Falls, Ontario, and notes on other occurrences. *Can. Mineral.* **2003**, *41*, 649–657. [[CrossRef](#)]
16. Dunkle, S.E.; Craig, J.R.; Lusardi, W.R. Romarchite and Associated Phases as Common Corrosion Products on Pewter Artifacts from Marine Archaeological Sites. *Geoarchaeology* **2004**, *19*, 531–552. [[CrossRef](#)]
17. Dubrovinskaia, M.; Messingschlager, M.; Dubrovinsky, L. Tin weathering experiment set by nature for 300 years: Natural crystals of the anthropogenic mineral hydromarchite from Creussen, Bavaria, Germany. *Eur. J. Mineral.* **2022**, *34*, 563–572. [[CrossRef](#)]
18. Strunz, H.; Nickel, E.H. *Strunz Mineralogical Tables—Chemical-Structural Mineral Classification System*, 9th ed.; Schweizerbart: Stuttgart, Germany, 2001.
19. Warr, L.N. IMA-CNMNC approved mineral symbols. *Miner. Mag.* **2021**, *85*, 291–320. [[CrossRef](#)]
20. Garuti, G.; Zaccarini, F. Minerals of Au, Ag and U in volcanic-rock-associated massive sulfide deposits of the northern Apennine ophiolite, Italy. *Can. Mineral.* **2005**, *43*, 935–950. [[CrossRef](#)]
21. Abrahams, I.; Grimes, S.M.; Johnston, S.R.; Knowles, J.C. Tin(II) Oxyhydroxide by X-ray Powder Diffraction. *Acta Crystallogr.* **1996**, *C52*, 286–288. [[CrossRef](#)]
22. Hill, R.J. Structure of $\text{Pb}_3\text{O}_2(\text{OH})_2$ by Rietveld Analysis of Neutron Powder Diffraction Data. *Acta Cryst.* **1985**, *C41*, 998–1003. [[CrossRef](#)]
23. Hahn, T. *International Tables for Crystallography Volume A—Space-Group Symmetry*, 4th ed.; Kluwer Academic Publishers: Dordrecht, The Netherlands, 1996.
24. Neumann, W.P.; König, K. Preparation and Structure of Diphenyltin. *Angew. Chem. Int. Ed.* **1962**, *1*, 212–213. [[CrossRef](#)]
25. Neumann, W.P.; König, K. Organozinnverbindungen, VIII. Über Diarylzinn-dihydride und Zinndiaryle mit höheren Arylresten. *Ann. Chem.* **1964**, *677*, 12–18. [[CrossRef](#)]
26. Neumann, W.P.; Pedain, J.; Sommer, R. Organozinnverbindungen, XIV Aliphatisch substituierte Cyclostannane. *Ann. Chem.* **1966**, *694*, 9–18. [[CrossRef](#)]
27. Puff, H.; Breuer, B.; Gehrke-Brinkmann, G.; Kind, P.; Reuter, H.; Schuh, W.; Wald, W.; Weidenbrück, G. Bindungsabstände zwischen organylsubstituierten Zinnatomen. III. Offenkettige Verbindungen. *J. Organomet. Chem.* **1989**, *363*, 265–280. [[CrossRef](#)]
28. Puff, H.; Bach, C.; Reuter, H.; Schuh, W. Bindungsabstände zwischen organylsubstituierten Zinnatomen. I. Cyclo-Hexastannane. *J. Organomet. Chem.* **1984**, *277*, 17–28. [[CrossRef](#)]
29. Bruker. *APEX 2—Suite of Crystallographic Software*, 5th ed.; Bruker AXS LLC: Madison, WI, USA, 2008.
30. Spek, A.L. Structure validation in chemical crystallography. *Acta Cryst.* **2009**, *D65*, 148–155. [[CrossRef](#)]
31. Spek, A.L. checkCIF validation ALERTS: What they mean and how to respond. *Acta Cryst.* **2020**, *E76*, 1–11. [[CrossRef](#)]

32. Mantina, M.; Chamberlin, A.C.; Valero, R.; Cramer, C.J.; Truhlar, D.G. Consistent van der Waals Radii for the Whole Main Group. *J. Phys. Chem. A* **2009**, *113*, 5806–5812. [CrossRef]
33. Clementi, E.; Raimondi, D.L.; Reinhardt, W.P. Atomic Screening Constants from SCF Functions. II. Atoms with 37 to 86 Electrons. *J. Chem. Phys.* **1967**, *47*, 1300–1307. [CrossRef]
34. Brese, N.E.; O’Keeffe, M. Bond-Valence Parameters for Solids. *Acta Cryst.* **1991**, *B47*, 192–197. [CrossRef]
35. Gagné, O.C.; Hawthorne, F.C. Comprehensive derivation of bond-valence parameters for ion pairs involving oxygen. *Acta Cryst.* **2015**, *B71*, 562–578. [CrossRef]
36. Brown, I.D. On the valence of bonds in the oxycomplexes of Sn^{2+} . *Acta Cryst.* **2009**, *B65*, 684–693. [CrossRef]
37. Krivovichev, S.V.; Brown, I.D. Are the compressive effects of encapsulation an artifact of the bond valence parameters? *Z. Krist.* **2009**, *216*, 245–247. [CrossRef]
38. Sidey, V. Alternative presentation of the Brown–Wu bond-valence parameters for some s^2 cation/ O^{2-} ion pairs. *Acta Cryst.* **2009**, *B65*, 99–101. [CrossRef]
39. Uglova, E.; Reichelt, M.; Reuter, H. Formation and structural characterization of the basic tin(II) fluoride, $\text{Sn}_9\text{F}_{13}\text{O}(\text{OH})_3 \cdot 2\text{H}_2\text{O}$, containing the unprecedented $[\text{Sn}_4\text{O}(\text{OH})_3]^{3+}$ cage-ion. *Z. Anorg. Allg. Chem.* **2022**, *648*, e2022003. [CrossRef]
40. Harrison, P.G.; Haylett, B.J.; King, T.J. X-ray Crystal Structure of $\text{Sn}_6\text{O}_4(\text{OMe})_4$: An Intermediate in the Hydrolysis of Tin(II) Dimethoxide. *J. Chem. Soc. Chem. Commun.* **1978**, 112–113. [CrossRef]
41. Suslova, E.V.; Turova, N.Y.; Kessler, V.G.; Belokon, A.I. Electrosynthesis of tin(II) alkoxides. *Russ. J. Inorg. Chem.* **2007**, *52*, 1682–1686. [CrossRef]
42. Hollingsworth, N.; Horley, G.A.; Mazhar, M.; Mahon, M.F.; Molloy, K.C.; Haycock, P.W.; Myers, P.; Critchlow, G.W. Tin(II) aminoalkoxides and heterobimetallic derivatives: The structures of $\text{Sn}_6(\text{O})_4(\text{dmae})_4$, $\text{Sn}_6(\text{O})_4(\text{OEt})_4$ and $[\text{Sn}(\text{dmae})_2\text{Cd}(\text{acac})_2]_2$. *Appl. Organomet. Chem.* **2006**, *20*, 687–695. [CrossRef]
43. Zöllner, T.; Iovkova-Berends, L.; Dietz, C.; Berends, T.; Jurkschat, K. On the Reaction of Elemental Tin with Alcohols: A Straight-forward Approach to Tin(II) and Tin(IV) Alkoxides and Related Tin-oxo Clusters. *Chem. Eur. J.* **2011**, *17*, 2361–2364. [CrossRef] [PubMed]
44. Boyle, T.J.; Alam, T.M.; Rodriguez, M.A.; Zechmann, C.A. Hydrolysis of Tin(II) Neo-pentoxide: Syntheses, Characterization, and X-ray Structures of $[\text{Sn}(\text{ONep})_2]_\infty$, $\text{Sn}_5(\mu_3\text{-O})_2(\mu\text{-ONep})_6$, and $\text{Sn}_6(\mu_3\text{-O})_4(\mu\text{-ONep})_4$ Where $\text{ONep} = \text{OCH}_2\text{CMe}_3$. *Inorg. Chem.* **2002**, *41*, 2574–2582. [CrossRef] [PubMed]
45. Boyle, T.J.; Doan, T.Q.; Steele, L.A.M.; Apblett, C.; Hoppe, A.M.; Hawthorne, K.; Kalinich, R.M.; Sigmund, W.M. Tin(ii) amide/alkoxide coordination compounds for production of Sn-based nanowires for lithium ion battery anode materials. *Dalton Trans.* **2012**, *31*, 9349–9364. [CrossRef] [PubMed]
46. Yanovsky, A.I.; Turova, N.Y.; Turevskaya, E.P.; Struchkov, Y.T. Entry BIBDEV in CCSD database. *Koord. Khimiia* **1982**, *8*, 153.
47. Clegg, W.; Elsegood, M.R.J. Echevarria CCDC 2034650: Experimental Crystal Structure Determination. *CSD Commun.* **2020**. [CrossRef]
48. Locock, A.J.; Ramik, R.A.; Back, M.E. The structures of two novel Sn^{2+} oxysalts found with Romarchite and Hydromarchite as corrosion products of pewter artifacts. *Can. Mineral.* **2006**, *44*, 1457–1467. [CrossRef]
49. Friedrich, E. Darstellung, Eigenschaften und Röntgenstrukturanalyse Diisopropylsubstituierter Zinn-Chalcogen-Verbindungen. Ph.D. Thesis, Universität Bonn, Bonn, Germany, 1984.
50. Neumann, W.P.; Burkhardt, G. Organozinnverbindungen, IV. Die Komproportionierung von Zinnalkylen mit Zinnhalogeniden und die Darstellung von Alkylzinn-Trihalogeniden. *Liebigs Ann. Chem.* **1963**, *663*, 11–21. [CrossRef]
51. Krause, L.; Herbst-Irmer, R.; Sheldrick, G.M.; Stalke, D. Comparison of silver and molybdenum microfocus X-ray sources for single-crystal structure determination. *J. Appl. Cryst.* **2015**, *48*, 3–10. [CrossRef]
52. Sheldrick, G.M. A short history of SHELX. *Acta Cryst.* **2015**, *C71*, 3–8. [CrossRef]
53. Brandenburg, K. *DIAMOND—Visual Crystal Structure Information System*; Crystal Impact GbR: Bonn, Germany, 1999.
54. POV-Ray—Persistence of Vision Raytracer, Version 3.6. 2004. Available online: <http://www.povray.org/download/> (accessed on 31 March 2023).

Disclaimer/Publisher’s Note: The statements, opinions and data contained in all publications are solely those of the individual author(s) and contributor(s) and not of MDPI and/or the editor(s). MDPI and/or the editor(s) disclaim responsibility for any injury to people or property resulting from any ideas, methods, instructions or products referred to in the content.